Helical Divertor and the Local Island Divertor in the Large Helical Device

S Masuzaki, T Morisaki, A Komori, N Ohyabu, H Suzuki, R Sakamoto, H Yamada, M Goto, S Morita, B J Peterson, K Narihara, K Tanaka, T Tokuzawa, K Kawahata, N. Noda, Y. Kubota, T Watanabe, Y Matsumoto*, O Motojima, J F Lyon**, C C Klepper**,

A C England**, LHD and CHS Experimental Groups

National Institute for Fusion Science, Oroshi-cho 322-6, Toki-shi, JAPAN 509-5292
Hokkaido university, Division of Quantum Energy Engineering, JAPAN 060-8628
Oak Ridge National Laboratory, Oak Ridge, Tennessee 37831, U.S.A.

Abstract. In the Large Helical Device, active edge plasma control using two types of divertor, helical divertor and the local island divertor, is planned, respectively. The former is intrinsic in the heliotron-type magnetic configuration. In the latter case, large pumping efficiency is expected by making particle recycling be localized toroidally using a divertor-head and an externally produced m=1, n=1 island. In this paper, the divertor properties in the helical divertor configuration are reviewed. The numerical result for design of local island divertor is described. The results of the local island divertor experiment performed in the Compact Helical System are also briefly reviewed.

1. Introduction

For the heliotron-type devices, plasma current is not essential to form magnetic configuration for plasma confinement, and thus, they have it without plasma, and do not suffer from disruption. Therefore, they have advantages over tokamaks from the point of view of steady state fusion plasma operation. Moreover, intrinsic divertor structure (helical divertor, HD) exists in the heliotron-type magnetic configuration without additional divertor coils. Unlike axisymmetric divertor in tokamaks, in this magnetic configuration, open field lines region exists between the last closed flux surface and X-point instead of clear separatrix. In the Large Helical Device (LHD), the largest superconducting heliotron-type device, plasma experiment under the HD configuration has been performed since 1998 [1-3]. One of the main issues in this experimental stage is understanding of the HD properties to design active particle control system using HD with appropriate baffles and pumping system.

On the other hand, another type of divertor configuration, the local island divertor (LID), is planned to apply to LHD to make clear the effects of particle pumping in a heliotron-type device [4, 5]. Particle outflux from the core is lead to a divertor head surrounded by a pumping duct through the separatrix of an externally produced m/n=1/1 island in periphery. A large pumping efficiency is expected in this configuration, and the main purpose is the investigation of the effects of neutral particle pumping on the confinement properties. The principle of the LID concept was proved by experiments in the Compact Helical System (CHS), a small size heliotron-type device [6-8]. The LID for the LHD experiment is being fabricated, and its experiment will be started in 2002.

In this paper, the physical understandings of HD in LHD, and the design of LID for LHD will be shown. The experimental results in the proof of the LID principle experiment in CHS are also described.

2. Helical divertor configuration in LHD

2.1. Edge and divertor Magnetic Structures in Helical Divertor (HD)

Complicated edge magnetic structure in the helical divertor configuration in LHD has been studied mainly using field line tracing calculation [9-11]. Figure 1 shows a schematic view of the HD configuration in LHD. The open field lines region which consists of three open field layers exists between the last closed flux surface (LCFS) and X-points instead of a clear separatrix. In Fig.1, with an increase of the minor radius, the poloidal mode number of the natural islands which exist in peripheral region decrease and the width of them increase. Eventually, the islands overlap, and the stochastic field structure appears (stochastic layer).

When the field lines in this region approach the X-point, they are folded and stretched by radial movement of X-point and high local rotational transform and shear on the torus outboard or inboard side. This generates multiple layers structure (edge surface layers).

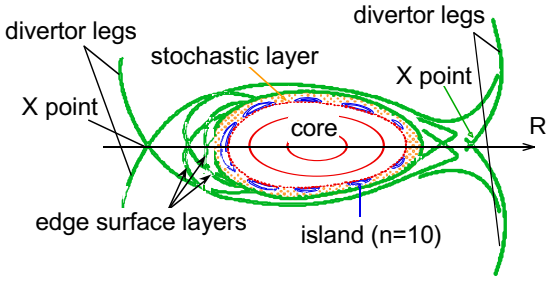

Figure 1. Scheme of the LHD magnetic configuration (horizontally elongated cross-section).

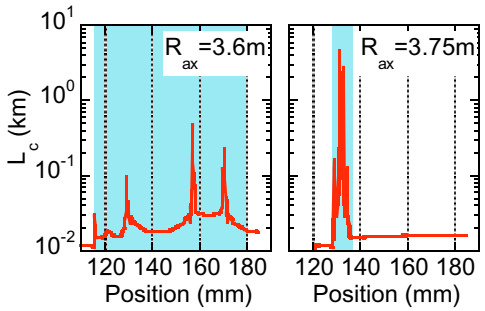

Figure 2. Profiles of the connection length (L_c) of the field lines connected to a torus inboard-side divertor plate for two magnetic axis positions (R_{ax}). Hatched regions are divertor legs.

At last, field lines of edge surface layers are connected to vacuum vessel (divertor plate). Figure 2 shows the profiles of the connection length (L_c) of the field lines connected to a divertor plate for two magnetic axis positions (R_{ax}). The divertor legs in Fig.1 correspond to the hatched region in Fig. 2. There are very long L_c peaks in the divertor legs. These long field lines come from the stochastic layer through the edge surface layers, and thus, they are the main channel of particle and heat outflux from the core. The field line structures at the divertor reflect that of edge surface layers. In the case of R_{ax}=3.6m, the structure is expanded. The peaks of long L_c and the flat region of short (a few tens meter) L_c appear alternately. The short field lines in divertor legs are not connected to stochastic layer, and come from outside of the stochastic layer. In the case of R_{ax}=3.75m, this structure converges. The region of very short (less than 20m) field lines appear by the divertor legs, and these short field lines exist outside of X-points. The minor radius of X-points are correspondent to that of the helical coils. Outside of this minor radius, the toroidal field component weakens, and thus, the direction of the field lines at the divertor plates almost poloidal. The length of field lines between X-points and the divertor plates is only several meters even the field lines with long L_c. In the HD configuration, the field line structure is three-dimensional, and the different L_c profiles appear at the different divertor plates.

The calculation of field line tracing including the effect of particle diffusion was conducted to predict the particle deposition profiles on HD which are three-dimensional [12]. Figure 3(a) shows results of the calculation for two R_{ax} cases. The particle deposition profiles, that is the divertor traces, shown as functions of toroidal and poloidal angles for one toroidal period (72 degree). The definitions of these angles are depicted in Fig.3(b). Three-dimensional particle deposition profiles appear in these figures. The particle deposition is not uniform in HD even in the helical direction. The profile depends on the magnetic configuration, such as R_{ax}. In the case of R_{ax}=3.6m, the particle deposition becomes maximum at torus inboard-side. On the other hand, it becomes maximum at top and bottom for R_{ax}=3.75m case.

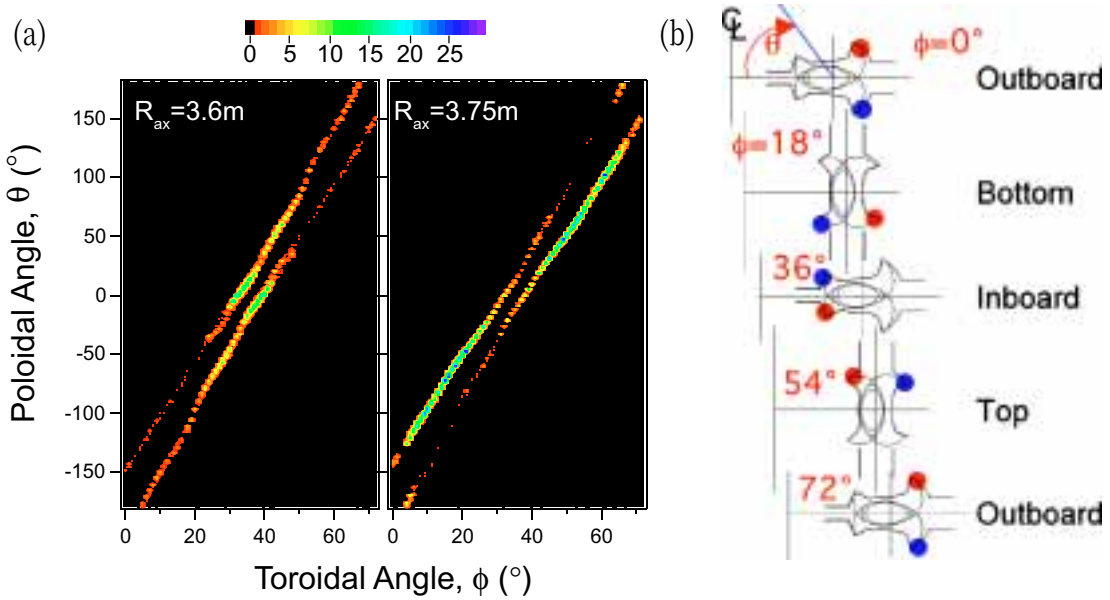

Figure 3. (a) Profiles of the particle deposition on the helical divertor (calculation) [13].
(b) The definition of toroidal and poloidal angle in (a) and poloidal cross-sections of plasma and vacuum vessel at the position.

2.2. Experimental results

The LHD is an l=2 heliotron-type device, and its device parameters are: the major radius, R=3.9m, the averaged minor radius, a=0.65m and the toroidal mode number of the helical coil, m=10. Operating magnetic axis and field strength are R_{ax}=3.5-3.9m and B=0.6-2.8 T, respectively. Main operating magnetic axis is R_{ax}=3.6m from the experiment in 1999 [14].Currentless plasmas are produced by ECH (82.6 and 84 GHz), sustained and auxiliary heated by negative ion based NBI (up to 5.2MW in FY2000). The plasma density is controlled by gas-puffing and/or fueling pellet injection. The central chord line averaged density, $\bar{n}_e$, is (0.5-6)×$10^{19}$$m^{-3}$ with gas-puffing, and up to 1.2×$10^{19}$$m^{-3}$ with pellet injection. Electron and ion temperature ranges are up to 4.4keV and 3.5keV, respectively.

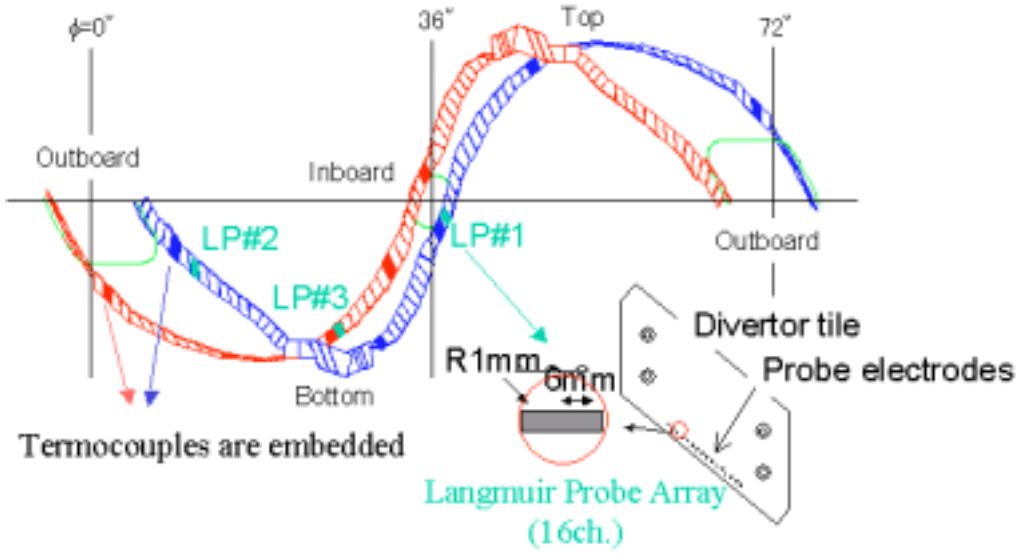

Figure 4. Diagnostics configuration for the divertor plasma. The definition of toroidal angle, ϕ, is same as Figure 3. The insertion is the scheme of the Langmuir probe array embedded in the divertor plates.

In this section, the experimental results concerning with the characteristics of the HD configuration in LHD are shown and discussed. The NBI heated and gas-puff fueled relatively low ⟨β⟩ (< 0.9 %) plasmas are mainly treated in this section, where ⟨β⟩ is the volume averaged β. The relatively high ⟨β⟩ (>2 %) plasmas and pellet fueled discharges are described in 2.2.3 and 2.2.4, respectively.

2.2.1. Particle flux and heat load to the divertor

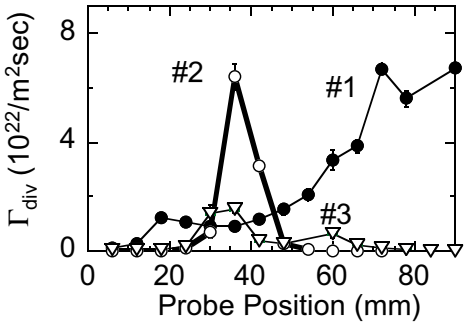

Figure 5. Profiles of the particle flux to the divertor plates (Γ_{div}). The positions of the plates are indicated #1-#3 [13].

Particle flux and heat load to the divertor were measured by the Langmuir probe arrays and thermocouples embedded in the divertor plates. Figure 4 shows the positions of them in the helical divertor in the experiment in 2000. Three Langmuir probe arrays have been embedded in the divertor plates at torus inboard-side (#1, ϕ=38°/θ= - 8°), outboard-side (#2, ϕ=11°/θ= - 155°) and bottom (#3, ϕ=21°/θ= - 49°). The electrodes of the Langmuir probe arrays are dome-type (2mm of diameter). Typical profiles of particle flux to these Langmuir probe arrays for R_{ax}=3.6m are shown in Figure 5. Unfortunately, #1 probe array could not cover full profile of particle flux. The difference of the profiles are caused by the difference of the L_c profiles. The $\bar{n}_e$ dependences of the ion saturation current (I_{is}) to these three arrays and the ratio of I_{is} to #1 and #3 arrays to that to #2 array are shown in Figures 6. I_{is} increase almost linearly at all arrays with an increase of $\bar{n}_e$, and the ratio does not depend on $\bar{n}_e$. That means the particle deposition profile on HD is not affected by $\bar{n}_e$. I_{is} to #1 probe array (torus inboard-side) is the maximum and that to #3 probe array (bottom) is the minimum in these three arrays, and this tendency is qualitatively consistent with the results of calculation (Figure 3(a)).

Figure 7 shows the profiles of the divertor plates temperature rise (ΔT), that is heat load to the

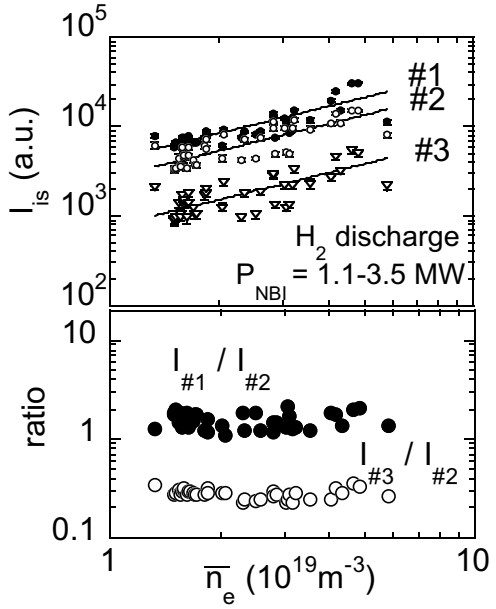

Figure 6. (a) Total ion saturation current (I_{is}) to the electrodes of #1-#3Langmuir probe arrays, and (b) The ratio of I_{is} to #1 and #3 arrays to I_{is} to #2 array, as functions of line averaged density [13].

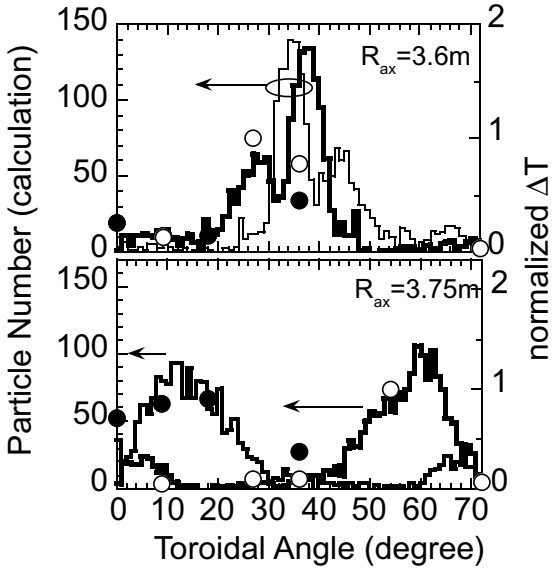

Figure 7. Profiles of temperature rises of the divertor plates (circles) and rewritten results of field line tracing (lines) for R_{ax}=3.6 and 3.75m [13]. Thin lines and closed circles correspond to the red divertor traces in Figure 3. Thick lines and open circles correspond to another traces.

divertor plates, measured by the thermocouples (see Figure 4) and rewritten field line tracing results (corresponds to Figure 3(a)) for R_{ax}=3.6m and 3.75m. The ΔT profiles show good agreement with the calculated particle deposition profiles. As mentioned previous section, long field lines, over several hundred meters, are the main channel of transfer particle and heat from LCFS to the divertor plates, and thus, these agreements between the field line tracing and experimental results are consistent.

2.2.2. Electron density and temperature in the divertor plasma

Electron density and temperature in the divertor plasma, $n_{e,div}$ and $T_{e,div}$, are measured using single probe characteristics. Figures 8 shows $n_{e,div}$ and $T_{e,div}$ versus $\bar{n}_e$, and electron density and temperature at LCFS, $n_{e,edge}$ and $T_{e,edge}$, are also plotted. The former is measured by Thomson scattering [15] and the latter is obtained by FIR interferometer with Abel inversion [16]. Both $n_{e,div}$ and $T_{e,div}$ decrease largely compared with $n_{e,edge}$ and $T_{e,edge}$. This result suggest that the plasma pressure is not conserved from the vicinity of LCFS to the divertor, and profiles of electron density and temperature in the open field lines region measured by Thomson scattering support that [13]. Ideally, stochastic field lines structure enhance the radial transport of particle and energy [17]. In LHD, the residual island structure exists near LCFS, and the ergodicity defined by Kolmogorov-length is small [11]. Therefore, in this region, radial transport is considered to be dominated by perpendicular transport to field lines rather than parallel one as in the closed surfaces region or axisymmetric divertor SOL in tokamaks. One of the different points between the open field lines region in the HD configuration and SOL in axisymmetric divertor tokamak is the connection length of field lines. The latter case, L_c is the order of πqR, where q is the safety factor, and it is over several hundred meters in the stochastic layer in LHD. Therefore collision with neutral particles and viscosity reduce the plasma pressure.

2.2.3. Divertor plasma in high β discharges

High β plasma experiments in LHD were performed with low magnetic field strength of 0.5-1.3T. With an increase of ⟨β⟩ value, the magnetic structure is modified. The position of magnetic axis shifts outward (Shafranov shift). Magnetic surfaces in periphery are destroyed, and the position of LCFS also move. Figure 9 shows

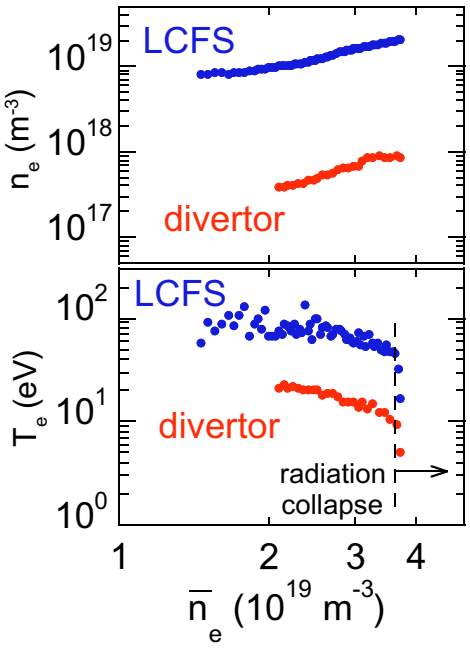

Figure 8. Electron density and temperature at LCFS and #2 probe array virsus line averaged density. P_{NBI}=1.5-1.7MW.

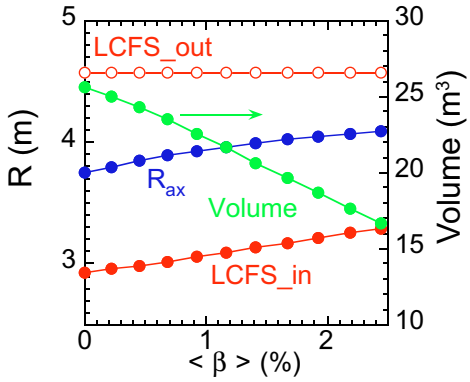

Figure 9. The positions of LCFS at the center chord of horizontally elongated cross-section, Shafranov-shift and plasma volume virsus ⟨β⟩.

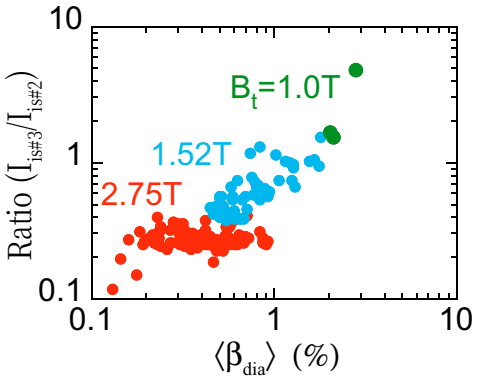

Figure 10. The ratio of Iis to #3 probe array (bottom) to that to #2 probe array (outboard) as a function of $\langle\beta_{dia}\rangle$.

the ⟨β⟩ dependence of the position of LCFS at horizontally elongated cross-section and the volume of closed surfaces region for the case of R_{ax}=3.75m. The inner position of LCFS moves outward, and the volume decreases with an increase of ⟨β⟩. The effects of such modification of the magnetic structure to the particle deposition on HD were investigated.

Figure 10 shows the ratio of I_{is} to #3 probe array (bottom) to that to #2 (outboard) probe array as a function of ⟨β⟩ for the operation with R_{ax}=3.6m. The ratio increases with an increase of ⟨β⟩ in the regime of ⟨β⟩ >0.9%. This result suggest that the particle deposition on HD is changed from that in the R_{ax}=3.6m operation to that in the outward shifted R_{ax} operations (R_{ax}>3.75m, see Figure 8). The profiles of ΔT of the divertor plates are shown in Figure 11. The change of the profile from that in low β operation to that in high ⟨β⟩ (~2%) operation is consistent with the Langmuir probe measurement (see Figures 8 and 10). Figure 12 shows Γ_{div} profiles on #2 and #3 Langmuir probe array in low and high β operations with initial R_{ax}=3.6m and in R_{ax}=3.75m operation. The positions of the divertor leg shift with change of R_{ax}, though they do not shift largely with β increase.

2.2.4. Divertor plasma in pellet fueled discharges

In LHD, pellet fueling experiments have been performed, and extension of the experimental regime has been achieved [18]. Figure 13 shows the maximum normalized plasma stored energy as a function of $\bar{n}_e$. The confinement degradation was observed in gas-puff fueled plasma at a density above $3.5\times10^{19}m^{-3}$. On the other hand, in the case of pellet fueled plasma, such confinement degradation has not been observed.

The profiles of electron density for gas-puff fueled plasma and pellet fueled plasma those have similar $\bar{n}_e$ are shown in Figure 14. In the former case, the profile is flat and is often accompanied by hollowness. On the other hand, the profile becomes peaked after the pellet injection [18, 19]. In contrast to the center density, peripheral density in pellet fueled plasma is lower, and hence the neutral density at this region is also lower than that in gas-puff case. Figure 15 shows $n_{e,div}$ and $T_{e,div}$ at #2 Langmuir probe array as functions of $\bar{n}_e$ in gas-puffing and pellet injection plasmas. At the same $\bar{n}_e$, low $n_{e,div}$ and high

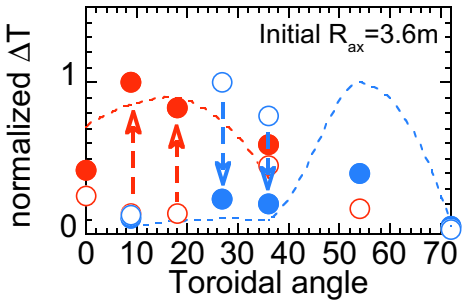

Figure 11. The change of the ΔT profile from that in low β operation to that in high β (⟨β_{dia}⟩ ~2%) operation (initial R_{ax}=3.6m). Open circles: low β, closed circles: high β, lines: envelopes of ΔT profile for Rax=3.75m and low β operation (see Figure 7).

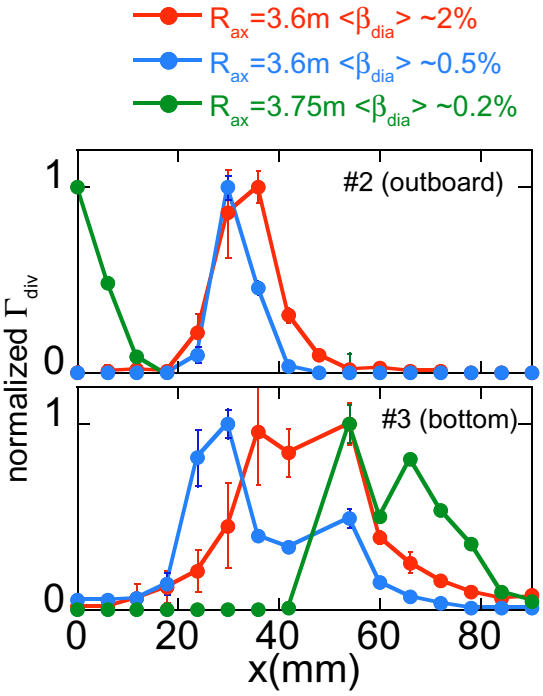

Figure 12. Profiles of particle flux to #2 and #3 divertor probe array in different operations.

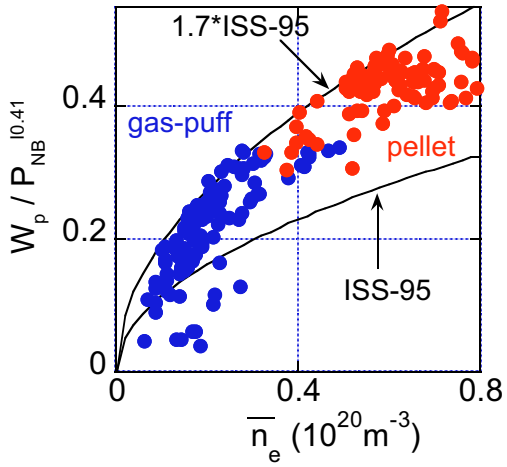

Figure 13. Maximum normalized stored energy versus line averaged density.

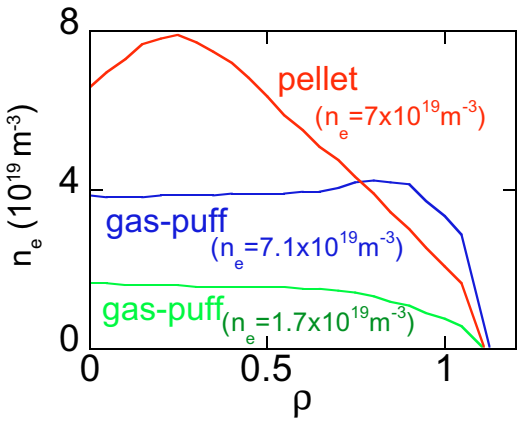

Figure 14. Profiles of electron density in gas-puff and pellet fueled plasmas. These profiles obtained by FIR interferometer with Abel inversion [16].

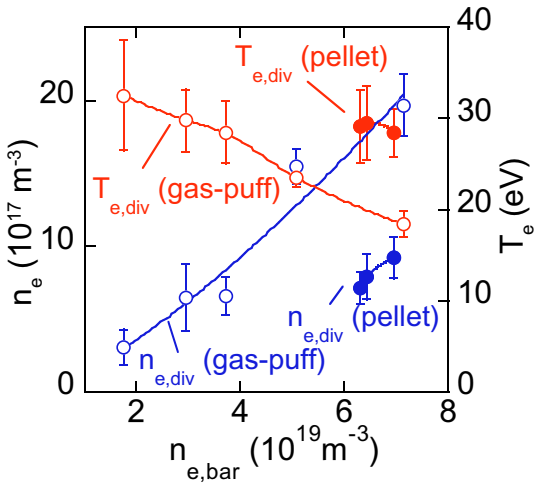

Figure 15. Electron density and temperature at the divertor in gas-puff and pellet fueled discharges, respectively (#2 probe array).

$T_{e,div}$ are observed in pellet fueled plasma. Particle flux to the divertor in pellet fueled discharge is smaller than gas-puff discharge, and thus, the particle recycling reduced. Figure 16 shows electron temperature at the divertor, vicinity of LCFS (ρ=0.97) and the pedestal (ρ=0.85) [20]. The high temperature region expands to peripheral region of the closed surface (ρ> ~0.85). In the region of ρ < ~0.85, T_e in pellet fueled plasma is lower than that in gas-puff fueled plasma.

At this stage, it is not clear why the experimental regime with good confinement is extended in pellet fueled plasma, and whether this regime can be further extended to higher density. One of the interesting points is whether the neutral density in peripheral region is a key parameter for the extension regime or not. This question is expected to be clear in the experiment with further high density, and with local island divertor.

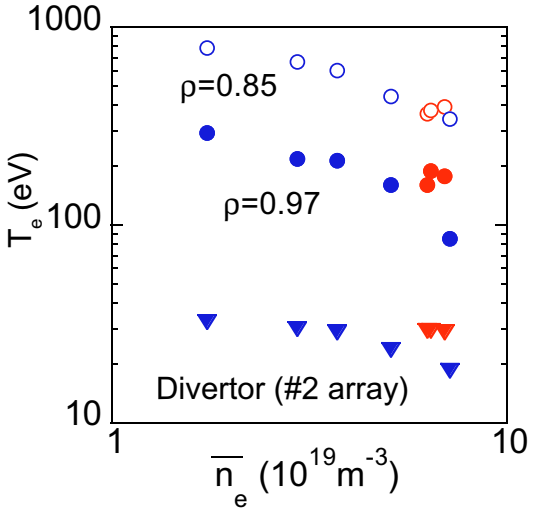

Figure 16. Electron temperature at the divertor (#2 probe array), vicinity of LCFS (ρ=0.97) and near pedestal (ρ=0.85) in gas-puff fueled (blue) and pellet fueled (red) discharges, respectively.

3. Local Island Divertor (LID) configuration

3.1. Local Island Divertor (LID)

Figure 15 depicts a schematic view of the LID configuration. An m/n=1/1 magnetic island externally produced by the perturbation field at the periphery of the closed surfaces region. A divertor head is inserted to the island from torus outboard-side. The outer separatrix of the island is connect to the back side of the head. Particle and heat outflux from the core strike the head, and

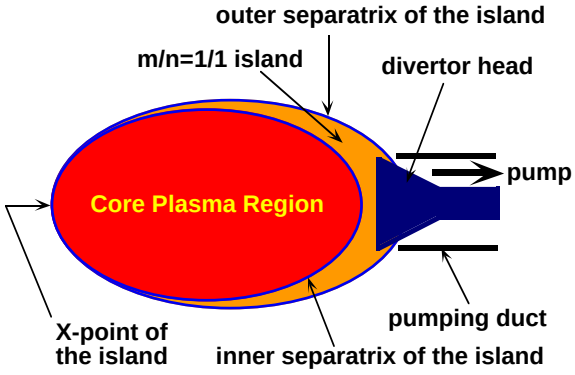

Figure 17. Scheme of the LID configuration.

thus, particle recycling localized in this region. A pumping duct surrounds the head to form a closed divertor system for efficient particle exhaust. The leading edge of the head is in the island to avoid the localized high heat load. With efficient pumping, the neutral pressure in the edge plasma region will be reduced, and hence the edge plasma temperature will be higher, hopefully leading to a better core confinement.

3.2. Proof of the Principle Experiment in CHS

To provide the principle of the LID concept, experiment with the LID configuration was performed in CHS, small heliotron-type device [6, 8, 21]. The device parameters of CHS are follows: major radius is 1.0m and averaged plasma minor radius is 0.2m, the toroidal magnetic field is 0.9T, respectively, and the magnetic axis was fixed at R=99.5cm in this experiment. The separatrix of the m/n=1/1 island formed by 8 pairs of additional coils was utilized for the LID configuration. The divertor head and pump duct was made by stainless-steel. A cryogenic pump (21000L/sec) was installed behind the divertor head for particle exhaust.

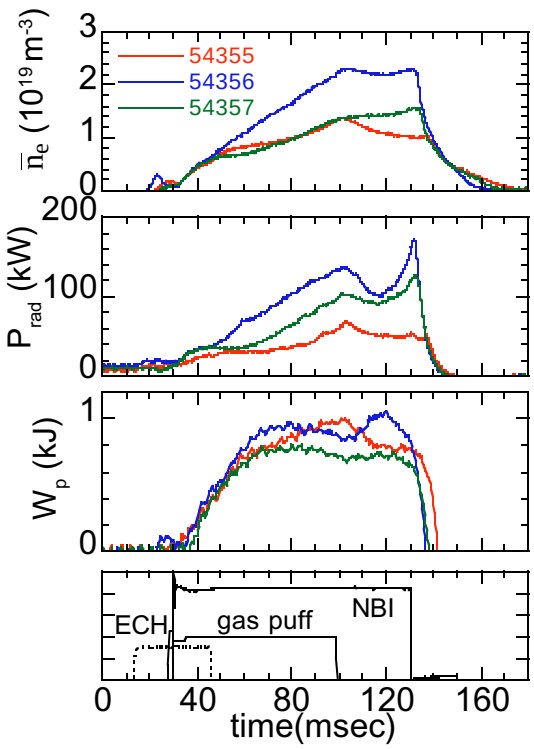

Figure 18. Typical time evolutions of (a) line averaged density, (b) radiation power, (c) stored energy. The same gas-puff rate was applied for #54355 (LID configuration) and #54356 (no LID configuration), and reduced gas-puff rate applied for #54357 (no LID configuration) [8].

3.2.1. Impact to Global Plasma Parameters

Figure 18 shows time evolutions of plasma parameters with and without LID configuration [8]. The line averaged density and radiation power reduced significantly with LID configuration with same gas-puffing rate. On the other hand, the stored energy was not changed. This result means that confinement modestly improved, and temperature rose in the confinement region [6]. The reduction of radiation loss is considered to be a primary reason for this temperature rise. The discharge of #54357 in Figure 18 was not LID configuration. With reduced gas-puffing rate in this discharge, the density was almost same as the discharge with LID configuration (#54355). The comparison of these two discharges indicates that the effect of LID configuration is not only reduction in density. The reduction of concentration of oxygen was observed, and this is considered to cause the reduced radiation loss [8].

3.2.2. Observations of Plasma Characteristics in front of the Divertor Head and Particle exhaust in the LID Configuration

At the divertor head, an ASDEX-type fast ion gauge measured neutral pressure in the pumping duct (P_{duct}) [21], and Langmuir probes embedded on the head measured the ion saturation current, electron density and temperature [22]. After particle flux coming to the divertor head, P_{duct} started to rise. The profile of ion saturation current indicates that the outer separatrix of the m/n=1/1 island led the particle flux well inside the pumping duct [22]. In the typical discharge with LID configuration ($\bar{n}_e$~1×10^{19}m^{-3}), the pumping rate, defined as the ratio of the neutral flux into the pumping duct (typically ~ 3 TorrL/sec, [21]) to the particle flux to the divertor head (typically ~ 1.6×10^{21} ions/sec [22]), was about 10-15 %. Both electron density and temperature just in front

of the head rose with forming the island [8]. The heat flux to the leading edge of the divertor head was well reduced compared with that in the discharges without the island [6].

3.3. Design of LID for LHD

The equipment for LID, such as the divertor head, the pumping duct and the pump system is under fabricating. By using eight cryogenic pumps with a hydrogen pumping speed of 42 m^3/sec, the effective pumping speed of 100 m^3/sec at the gate valve between LHD and the LID chamber will be achieved.

The width of the island is about 20 cm. In CHS, there is no closed surface outside the m/n=1/1 island but the open ergodic layer, and thus, the particle flux led to the divertor head was roughly about 20% of total outflux from the core. In LHD, the island formed well inside the closed surface region, and large portion of total outflux is expected to be led to the divertor head. Therefore, very efficient particle exhaust can be expected. Numerical results support these expectations. Figure 19 shows the ratio of the particle flux striking the divertor head to total outflux from the core as a function of the effective diffusion coefficient (D^*) obtained by the field line tracing including the diffusion [23]. More than 80 % of the ratio is achieved at the regime of D^* of smaller than 1 m^2/s. The analysis of the density profile in LHD using FIR interferometer, the diffusion coefficient is less than 1 m^2/s [16], and thus the assumed D^* is considered to be reasonable. Figure 20 shows the pumping efficiency (ε_{pump}) as a function of the electron density in the plasma in front of the divertor head calculated by DEGAS code with simple assumptions [23]. The definition of ε_{pump} is the ratio of the number of the pumped particles to total number of particles. About ε_{pump}=20% is achieved at $n_e=1\times10^{19}m^{-3}$ and T_e=8.7eV. In Figure 20, ε_{pump} decreases with rises of n_e and T_e for increasing of the portion of ionization in front of the divertor head. The portion of escaped particle from the slit between the divertor head and pumping duct is about 10%. The ionized particles are not tracked in this calculation, however, the large ionization in front of the divertor head should lead the plasma regime to the high recycling or divertor detachment in experiment.

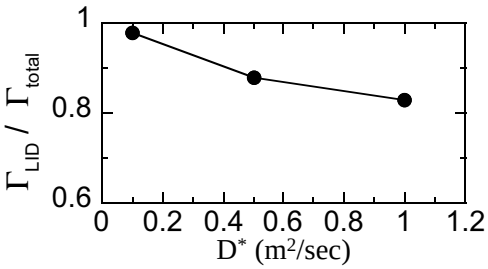

Figure 19. Collecting efficiency of particles by LID [23]. $\Gamma_{total}=\Gamma_{LID}+\Gamma_{HD}$, where Γ_{HD} is particle flux to helical divertor.

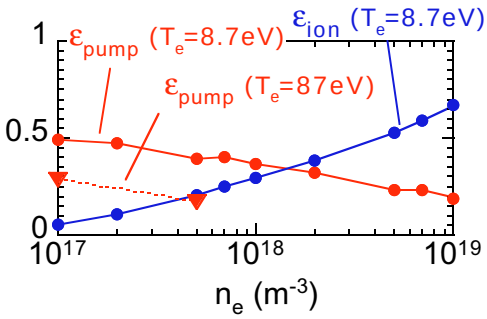

Figure 20. Pumping and ionzed efficiency of LID as functions of electron density in the plasma in front of the divertor head.

The concentrated particle flux to the divertor head bring also the concentrated heat flux. In LHD, the divertor head is covered by water cooled carbon plates. It's size is about 1 m×0.6 m, and the wet area will be > ~0.3m^2. The maximum steady state heat flux which the divertor head can withstand is at least 5 MW/m^2 in design.

4. Summary

The physical understandings of the plasma in the helical divertor in LHD are described. The complicated magnetic structure in the open field lines region dominate the profiles of plasma parameters in this region and in the helical divertor. Three-dimensional particle deposition on the helical divertor is predicted from numerical results, and experimental results is consistent with them. The sign of high recycling or divertor detachment have not observed.

The local island divertor experiment is planned in LHD to clarify the effect of the strong

pumping on plasma performance. This configuration also provides the sharp boundary in contrast to the helical divertor configuration. The basic functions of LID were confirmed in the experiment in CHS, and a modest improvement of the confinement was observed. The equipments for LID in LHD are now under fabricating. Numerical results show that a large pumping efficiency will be achieved.

References

[1] Iiyoshi A et al 1999 *Nucl. Fusion* **39** 1245.
[2] Motojima O et al 1999 *Phys. Plasma* **6** 1843.
[3] Fujiwara M et al 1999 *Plasma Phys. Control. Fusion* **41** B157.
[4] Ohyabu N et al 1987 *J. Nucl. Mater.* **145-147** 967.
[5] Komori A et al 1998 *J. Plasma Fusion Res.* **1** 398.
[6] Komori A et al 1996 *Proc. Plasma Physics and Controlled Nuclear Fusion Research* Montreal IAEA-CN-64/C1-2.
[7] Morisaki T et al 1997 *J. Nucl. Mater.* **241-243** 977.
[8] Masuzaki S et al 1998 *J. Plasma Fusion Res.* **1** 310.
[9] Akao H 1990 *J. Physical Society of Japan* **39** 1633.
[10] Ohyabu N 1994 *Nucl. Fusion* **34** 387.
[11] Morisaki T et al 2000 *Proc.27th EPS Conf. Controlled Fusion Plasma Phys. (Budapest, Hungary)* Vol.24B 780.
[12] Morisaki T et al 2000 *Contrib. Plasma Phys.* **40** 266.
[13] Masuzaki S et al under submission.
[14] Yamada H et al 2001 *Nucl. Fusion* **41** 901.
[15] Narihara K et al 2000 *Proc. 18th IAEA conference, Sorrento* EXP5/28.
[16] Tanaka K et al 2000 *Rev. Sci. Instrum.* **72** 1089.
[17] Gendrich Ph et al 2001 *J. Nucl. Mater.* **290-293** 798.
[18] Sakamoto R et al 2001 *Nucl. Fusion* **41** 381.
[19] Yamada H et al 2000 *Fusion Eng. Des.* **49-50** 915.
[20] Ohyabu N et al 2000 *Phys. Rev. Lett.* **84** 103.
[21] Lyon J et al 1997 *Proc.24th EPS Conf. Controlled Fusion Plasma Phys. (Berchtesgade, Germany)* Vol.21A 777.
[22] Masuzaki S et al 1997 *Proc.24th EPS Conf. Controlled Fusion Plasma Phys. (Berchtesgade, Germany)* Vol.21A 821.
[23] Morisaki T et al 2000 *J. Plasma Fusion Res.* **3** 188.